Supplemental Figure TOC

Figure S1. Acentrosomal cells have no apparent defects in interphase MTs or apical-basal polarity (related to Fig1). These data follow the observations regarding increased cell death in *sas-4* mutant wing discs presented in Fig1, and reveal that acentrosomal cells do not possess gross defects in the microtubule cytoskeleton or apicobasal polarity.

Figure S2. Dynamics of spindle assembly in wildtype and acentrosomal wing disc cells (related to Fig2). Still images from Supplemental Movies 1 and 2 demonstrating differences in microtubule nucleation and spindle assembly in wing discs with and without centrosomes, similar to the fixed images shown in Fig2.

Figure S3. RNAi effectively knocks down targeted genes (related to Fig3 and Fig7). Antibody staining of proteins encoded by genes that were RNAi targets demonstrates on-target effects of various lines.

Figure S4. Acentrosomal cells rely on the Augmin complex for cell viability and proper wing development (related to Fig3). Similar to codepletion of Sas-4 and Dgt2 (Fig3), knockdown of Sas-4 and Dgt3, Dgt4, or Dgt6 results in increased apoptosis and wing defects.

Figure S5. Adult wing phenotypes support genetic interaction between RCC1 and Sas-4 (related to Fig3). To bypass lethality associated with Rcc1 knockdown using ap-Gal4, we used the wing disc specific MS1096-Gal4 to attain adult wings for evaluating genetic interaction. Rcc1 knockdown alone causes significant wing defects and adding Sas-4 knockdown enhances these.

Figure S6. Blocking apoptosis in acentrosomal cells disrupts wing development and leads to increased expression of Wg and MMP1 (related to Fig6). Here we use an alternate Gal-4 driver to that described in Fig6 to bypass lethality and show that blocking cell death in wing cells lacking centrosomes disrupts adult wing morphology. Blocking cell death associated with loss of centrosomes leads to increased expression of Wg and MMP1.

Figure S7. Confirming genetic interaction between between Mud and additional centriole duplication factors and Mud knockdown leads to JNK-dependent apoptosis (related to Fig7). Similar to codepletion of Mud and Sas-4, double knockdown of Mud and Asl or Sas-6 increases the rates of apoptosis and adult wing phenotypes, and use of a second RNAi line targeting Mud also enhances Sas-4 related phenotypes. JNK mediates apoptosis due to *mud* knockdown.

Movie S1. Spindle assembly initiates from centrosomes in wildtype wing disc cells. Stills from this movie are shown in Fig S2.

Movie S2. In acentrosomal cells, spindle microtubules initiate around chromatin. Stills from this movie are shown in Fig S2.

Supplemental Data

Supplemental Figures

Figure S1. Acentrosomal cells have no apparent defects in interphase MTs or apical-basal polarity (related to Fig1). (A) Cross sectional view of a wildtype disc shows the apical and basal enrichments typical of interphase MTs in these cells. (B) We observed no appreciable difference in this MT distribution in *sas-4* mutant discs. (C) In the folds of wildtype discs, we can observe the apical accumulation of aPKC (red) and the basolateral localization of Dlg (green). (D) These patterns appear unaffected in *sas-4* mutant cells. Scale bars A-B=10mm, C-D=50mm.

Figure S2. Dynamics of spindle assembly in wildtype and acentrosomal wing disc cells (related to Fig2). Stills from live-imaging of a wildtype wing disc expressing the MT marker Jup:GFP and the chromatin marker His:RFP. A cell in mitotic prophase (0s; yellow arrows) shows MT nucleation at centrosomes (arrows), while the cell below segregates its chromosomes (red arrowhead). (H) In *sas-4* mutant discs, no MT nucleation activity is apparent at prophase (0s; red arrowhead). After NEB (320s), MTs begin to assembly around the chromatin (yellow arrow), and eventually form a spindle (920s); the spindle in the image shown is slightly off angle, thus the lower pole is not visible.

Figure S3. RNAi effectively knocks down targeted genes (related to Fig3 and Fig7). (A) sas-4 RNAi driven by ap>GFP in the dorsal wing compartment reduces Sas-4 protein levels, as indicated by anti-Sas-4 staining. Similar results are seen for RNAi targets, Mud (B) and Pins (C).

Figure S4. Acentrosomal cells rely on the Augmin complex for cell viability and proper wing development (related to Fig3). (A,C,E,G) Knockdown of Augmin components Dgt3, Dgt4, or Dgt6 does not result in elevated apoptosis or adult wing defects. (B,D,F,G) However, coexpressing *sas-4* RNAi and RNAi against any of these Augmin components results in a dramatic increase in apoptosis and wing defects.

Figure S5. **Adult wing phenotypes support genetic interaction between RCC1 and Sas-4 (related to Fig3).** To avoid the lethality associated with expression of *RCC1* RNAi using ap>Gal4, we used the tissue specific MS1096-Gal4 to drive *RCC1* RNAi in the wing disc, allowing recovery of adult wings. (A) While expression of *sas-4* RNAi alone did not obviously disrupt wing morphology, knockdown of RCC1 did lead to significant defects in adult wings (B). (C) Coexpression of *RCC1* and *sas-4* RNAi enhanced the wing phenotype, consistent with the increased apoptosis we observed in this genotype (see main Fig 3F,G).

Figure S6. Blocking apoptosis in acentrosomal cells disrupts wing development and leads to increased expression of Wg and MMP1 (related to Fig6). (A,B) Wings from males with MS1096-Gal4 driving *sas-4* RNAi or p35. These have minimal effect on adult wings. (C) In contrast, expressing p35 and *sas-4* RNAi, which blocks the apoptosis caused by *sas-4* RNAi, leads to dramatically disrupted wings. (D-G) Using *en>RFP* to drive the anti-apoptotic gene *p35* in the posterior compartment of a homozygous *sas-4* mutant wing disc leads to massive accumulation of Wg and MMP1 (green) in the posterior compartment.

Figure S7. Confirming genetic interaction between between Mud and additional centriole duplication factors and Mud knockdown leads to JNK-dependent apoptosis (related to Fig7). To verify the genetic interaction of *mud* with *sas-4,* we used double knockdown of Mud and either Asl or Sas-6, along with a separate *mud* RNAi line (28074). (A-F) While knockdown of Mud, Asl, or Sas-6 alone had only moderate effects on apoptosis rates (A,B,D,F), codepletion of Mud and either Asl (C) or Sas-6 (E), lead to increased cell death (F) and dysmorphic adult wings. Surprisingly, knockdown of Sas-6 alone has rather severe effects on adult wing (D”), though the double knockdown appeared worse (E”). (G-K) While knockdown of Mud using the new RNAi line had only moderate effects on apoptosis rates (G,K) and no effect on wing morphology (I), codepletion of Mud and Sas-4 led to increased cell death (H,K) and dysmorphic adult wings (J), thus recapitulating the genetic interaction with *sas-4* reported in the main text for *mud* RNAi line 35044. (K) Quantification of apoptosis levels in the two different *mud* RNAi lines used, with and without *sas-4* RNAi coexpression. Images and p-values for the *mud* RNAi (35044) line can be found in main Figure 7. (L) The increase in apoptosis associated with knockdown of Mud (using the stronger 35044 line) can be completely repressed by blocking JNK signaling through coexpression of bskDNScale bars=20mm.

Supplemental movies.

Movie S1 (Stills from this movie are shown in Fig S2). Live imaging of control wing disc (pouch region) expressing the microtubule (MT) marker Jupiter:GFP (Jup:GFP) and the chromosomal marker His2Av:RFP (His:RFP). In these wildtype cells, strong MT nucleation initiates at the pair of centrosomes during prophase, and spindle MTs can be seen extending from the centrosomes to the chromosomes. Frame rate=10fps.

Movie S2 (Stills from this movie are shown in Fig S2). Live imaging of a *sas-4* mutant disc (pouch region) expressing Jup:GFP and His:RFP. In contrast to wildtype, acentrosomal cells initiate spindle MT assembly around the chromosomes. The MTs appear to grow outward and eventually coalesce to form a relatively well-focused spindle. Note the long delay at metaphase in acentrosomal cells. Frame rate=10fps.

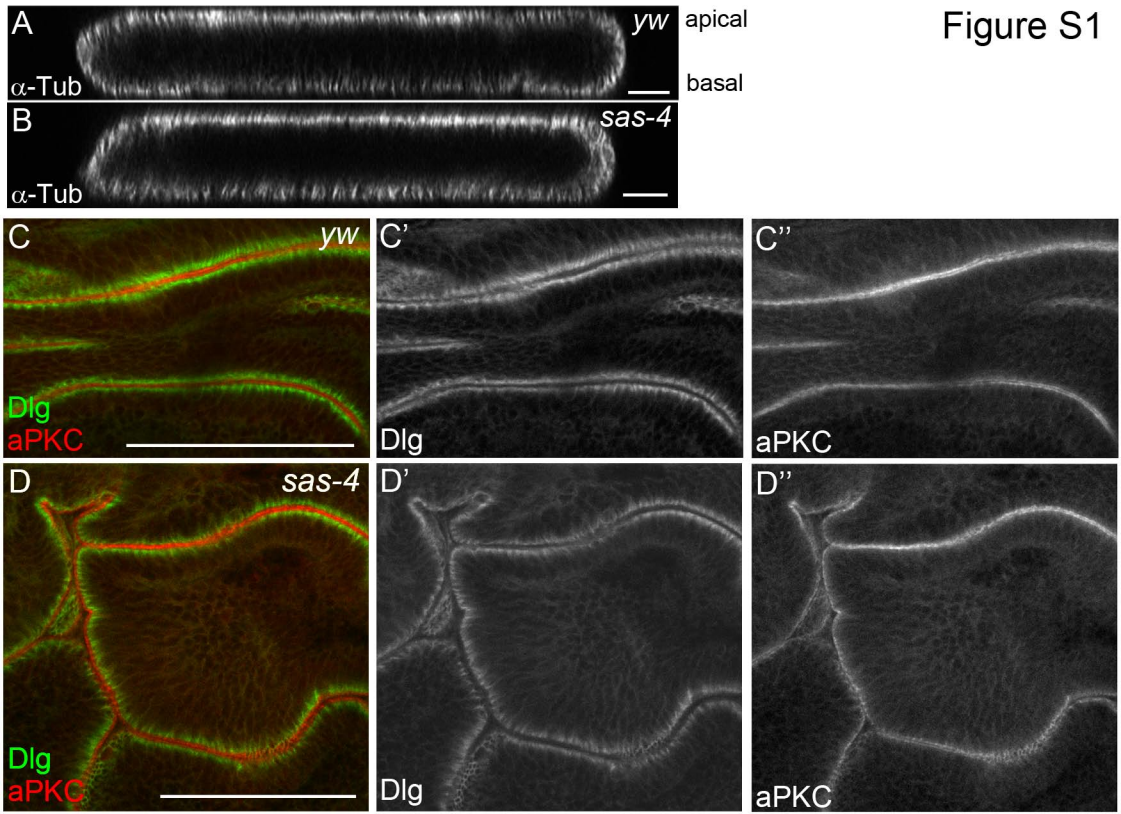
A
yw
apical
α-Tub
basal
B
sas-4
α-Tub
C
yw
C'
C''
Dlg
aPKC
Dlg
aPKC
D
sas-4
D'
D''
Dlg
aPKC
Dlg
aPKC

Figure S1

Figure S2

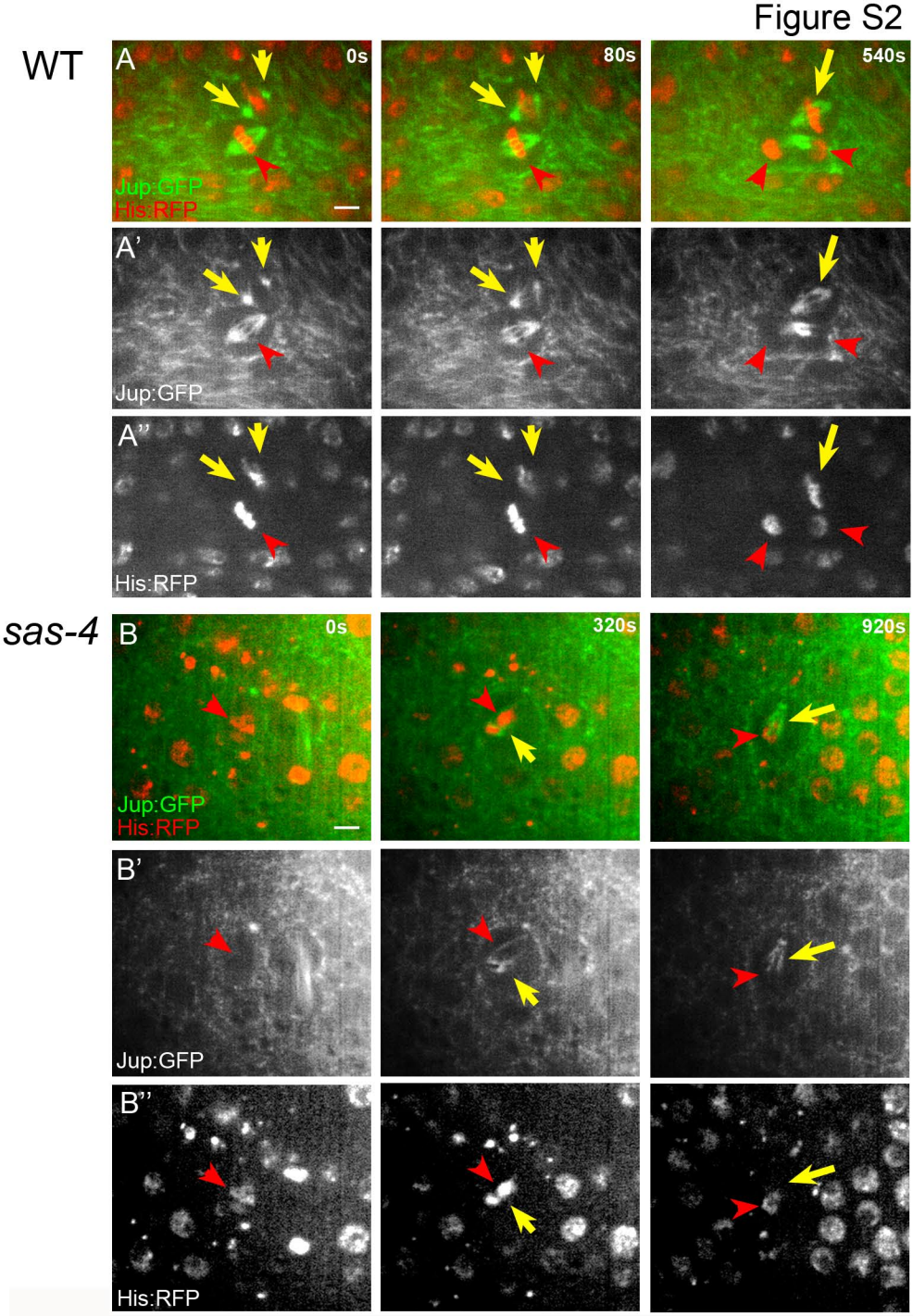
WT
A
0s
80s
540s
Jup:GFP
His:RFP
A'
Jup:GFP
A''
His:RFP
sas-4
B'
0s
320s
920s
Jup:GFP
His:RFP
B'
Jup:GFP
B''
His:RFP

Figure S3

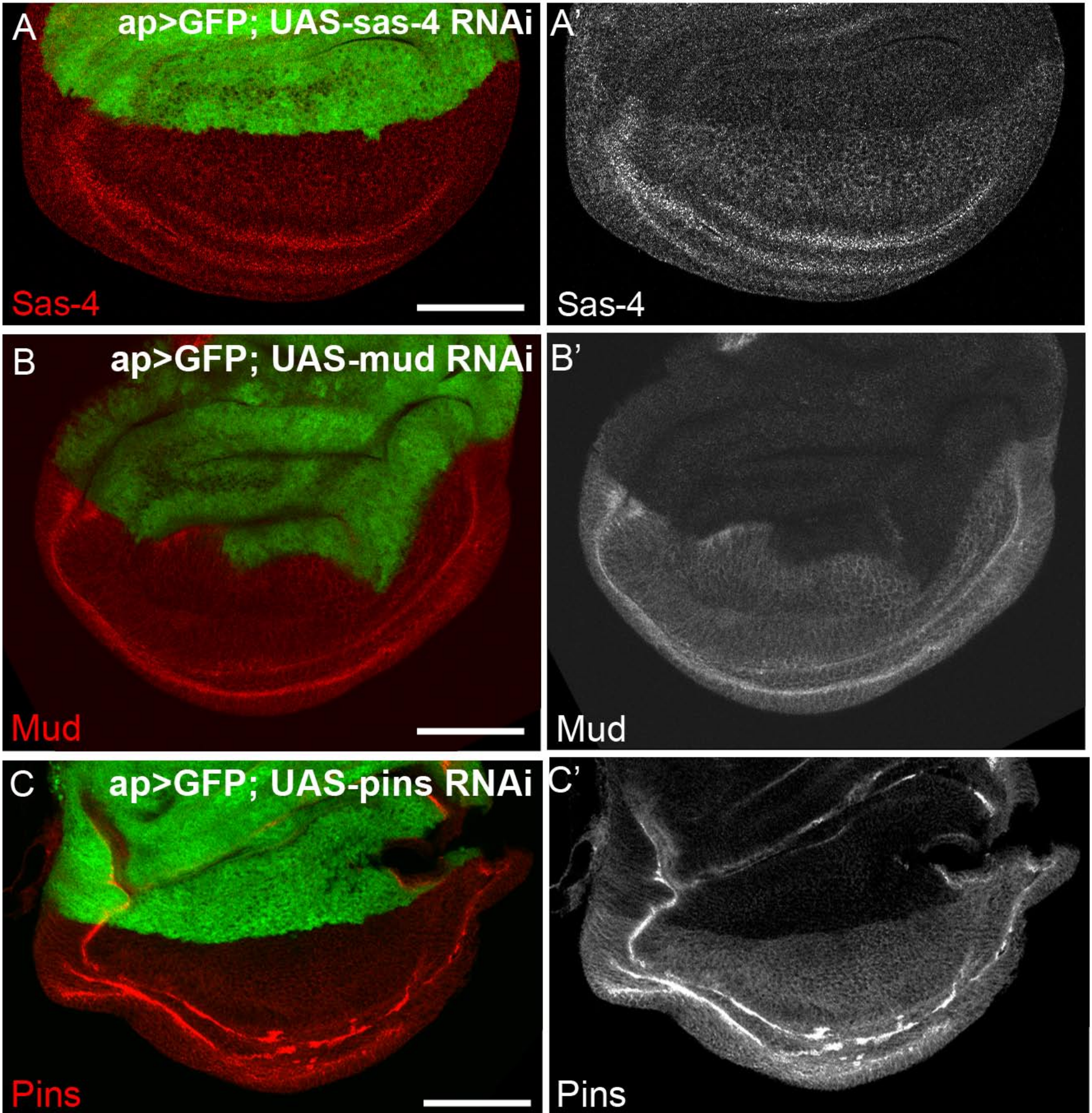
A
ap>GFP; UAS-sas-4 RNAi
Sas-4
A'
Sas-4
B
ap>GFP; UAS-mud RNAi
Mud
B'
Mud
C
ap>GFP; UAS-pins RNAi
Pins
C'
Pins

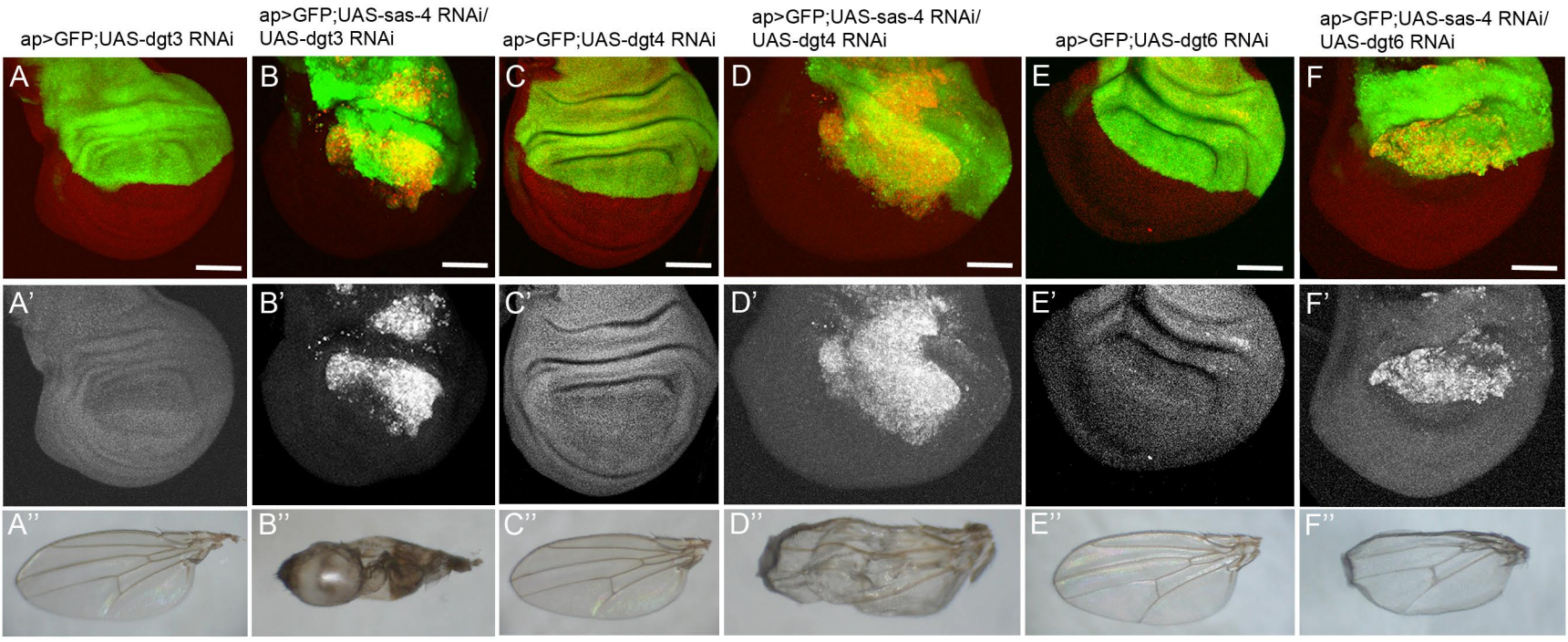
ap>GFP;UAS-dgt3 RNAi
ap>GFP;UAS-sas-4 RNAi/ UAS-dgt3 RNAi
ap>GFP;UAS-dgt4 RNAi
ap>GFP;UAS-sas-4 RNAi/ UAS-dgt4 RNAi
ap>GFP;UAS-dgt6 RNAi
ap>GFP;UAS-sas-4 RNAi/ UAS-dgt6 RNAi
A
B
C
D
E
F
A'
B'
C'
D'
E'
F'
A''
B''
C''
D''
E''
F''

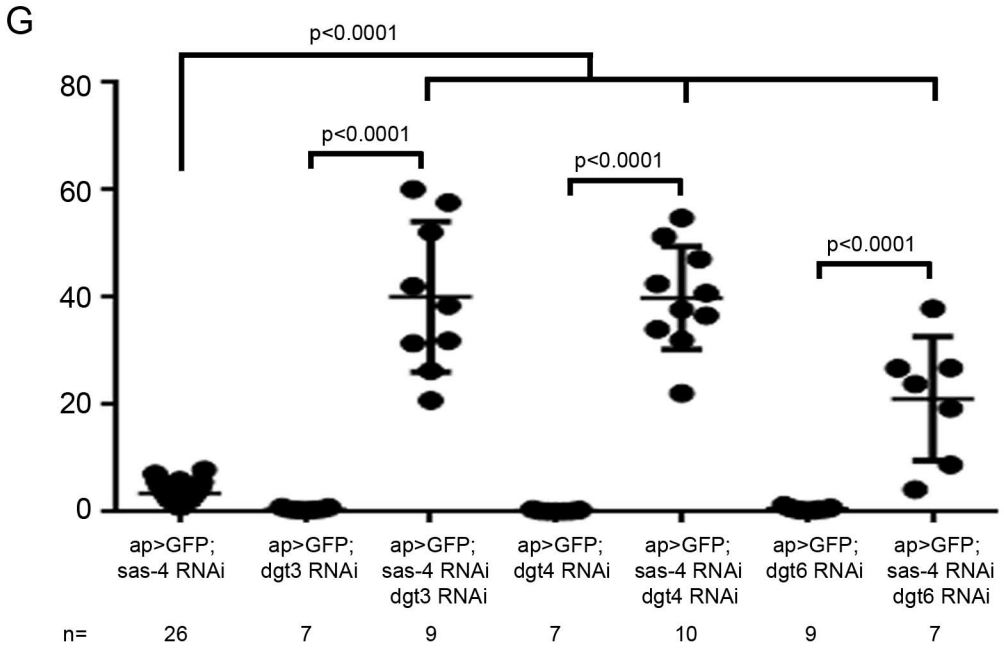
G
p<0.0001
p<0.0001
p<0.0001
p<0.0001
80
60
40
20
0
ap>GFP; sas-4 RNAi
ap>GFP; dgt3 RNAi
ap>GFP; sas-4 RNAi dgt3 RNAi
ap>GFP; dgt4 RNAi
ap>GFP; sas-4 RNAi dgt4 RNAi
ap>GFP; dgt6 RNAi
ap>GFP; sas-4 RNAi dgt6 RNAi
n=
26
7
9
7
10
9
7

Figure S4

MS1096-Gal4/+;;UAS-sas-4 RNAi

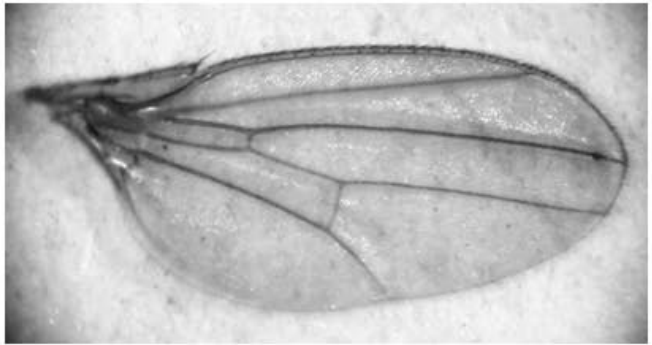

MS1096-Gal4/+;;UAS-Rcc1 RNAi

MS1096-Gal4/+;;
UAS-sas-4 RNAi/UAS-Rcc1 RNAi

Figure S5

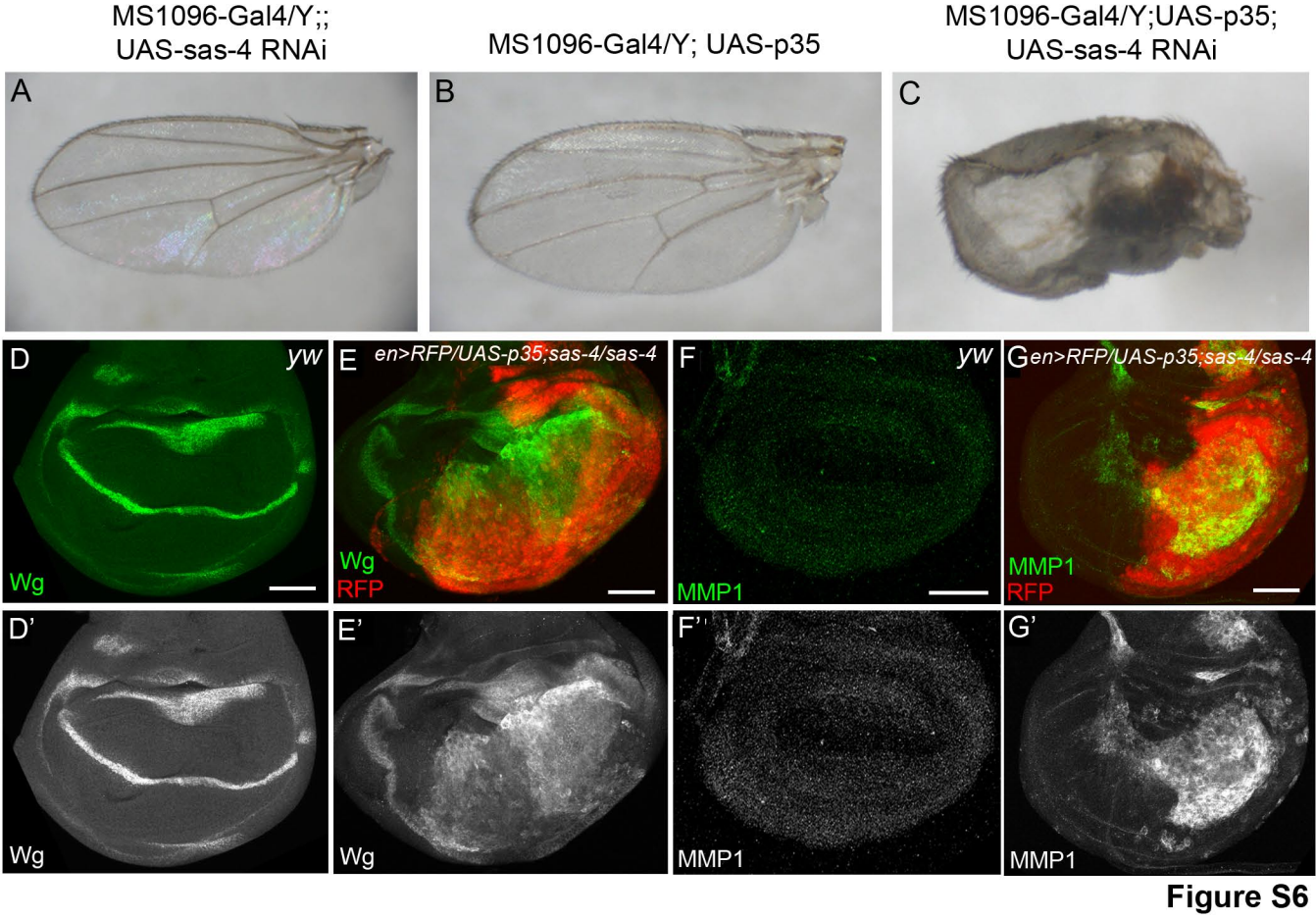
MS1096-Gal4/Y;;
UAS-sas-4 RNAi
MS1096-Gal4/Y; UAS-p35
MS1096-Gal4/Y;UAS-p35;
UAS-sas-4 RNAi
A
B
C
D
yw
Wg
E
en>RFP/UAS-p35;sas-4/sas-4
Wg
RFP
F
yw
MMP1
G
en>RFP/UAS-p35;sas-4/sas-4
MMP1
RFP
D'
Wg
E'
Wg
F'
MMP1
G'
MMP1

Figure S6

Figure S7

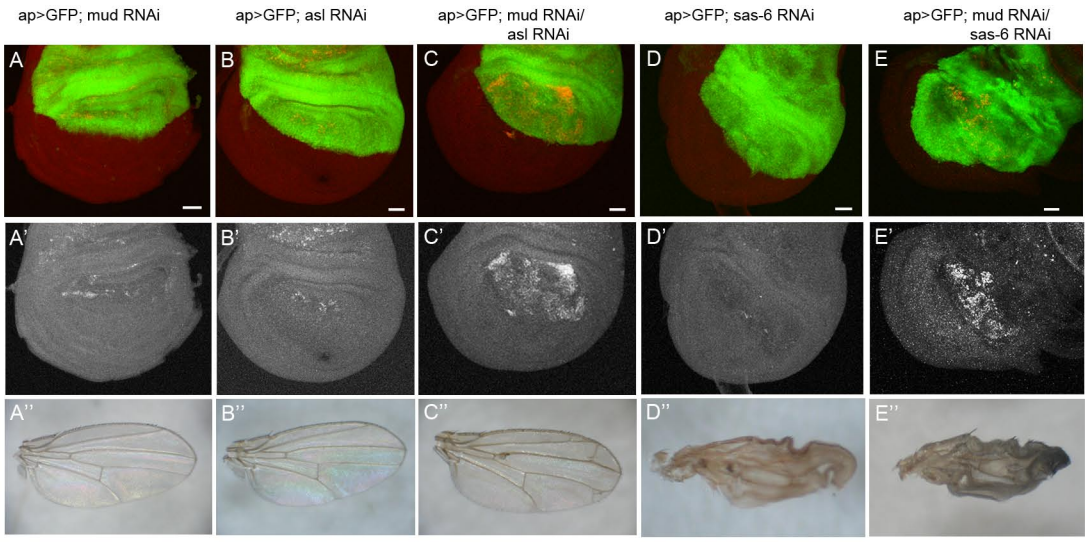
ap>GFP; mud RNAi
ap>GFP; asl RNAi
ap>GFP; mud RNAi/ asl RNAi
ap>GFP; sas-6 RNAi
ap>GFP; mud RNAi/ sas-6 RNAi
A
B
C
D
E
A'
B'
C'
D'
E'
A''
B''
C''
D''
E''

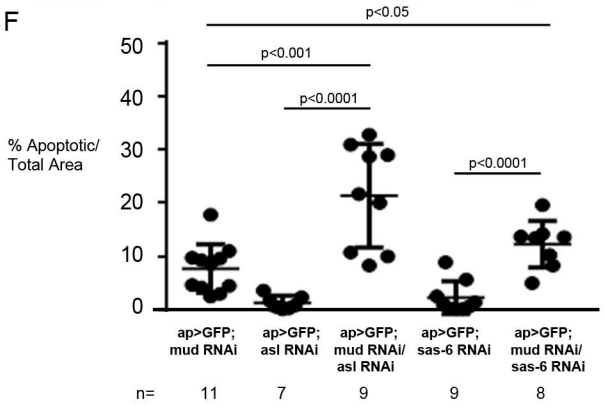
F
p<0.05
p<0.001
p<0.0001
p<0.0001
% Apoptotic/ Total Area
50
40
30
20
10
0
ap>GFP; mud RNAi
ap>GFP; asl RNAi
ap>GFP; mud RNAi/ asl RNAi
ap>GFP; sas-6 RNAi
ap>GFP; mud RNAi/ sas-6 RNAi
n=
11
7
9
9
8

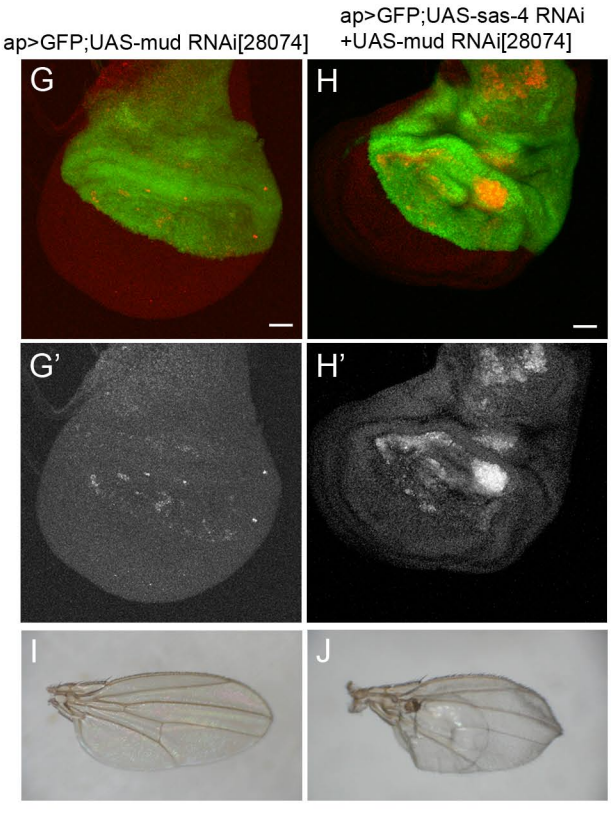
ap>GFP;UAS-mud RNAi[28074]
ap>GFP;UAS-sas-4 RNAi +UAS-mud RNAi[28074]
G
H
G'
H'
I
J

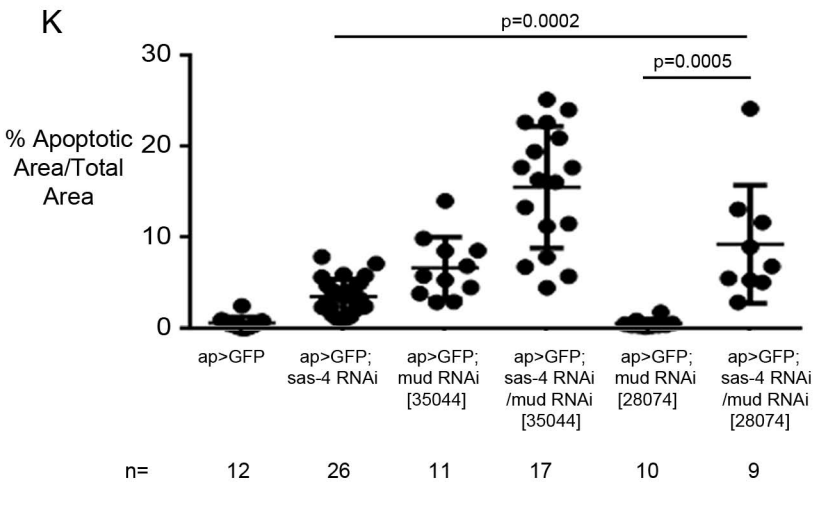
K
p=0.0002
p=0.0005
% Apoptotic Area/Total Area
30
20
10
0
ap>GFP
ap>GFP; sas-4 RNAi
ap>GFP; mud RNAi [35044]
ap>GFP; sas-4 RNAi /mud RNAi [35044]
ap>GFP; mud RNAi [28074]
ap>GFP; sas-4 RNAi /mud RNAi [28074]
n=
12
26
11
17
10
9

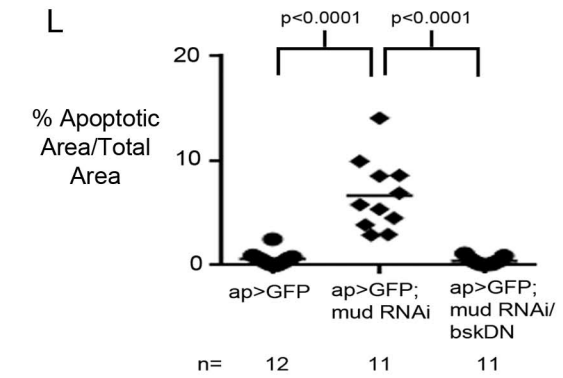
L
p<0.0001
p<0.0001
% Apoptotic Area/Total Area
20
10
0
ap>GFP
ap>GFP; mud RNAi
ap>GFP; mud RNAi/ bskDN
n=
12
11
11

Supplemental Experimental Procedures

Fly stocks	Source
y w	Bloomington Stock Center #1495 (IN, USA)
sas-4^{S2214}	Bloomington Stock Center #12119
cnn^{HK21}	Bloomington Stock Center #5039
UAS-sas-4 RNAi	Bloomington Stock Center #35049
UAS-dgt2 RNAi	Bloomington Stock Center #31729
UAS-mud RNAi	Bloomington Stock Center #35044,28074
UAS-pins RNAi	Bloomington Stock Center #35048
UAS-p53[H159N]	Bloomington Stock Center #8421
UAS-p53[R155H]	Bloomington Stock Center #8419
UAS-p35	Bloomington Stock Center #5072
en-GAL4 UAS-RFP	Bloomington Stock Center #30557
MS1096-GAL4	Bloomington Stock Center #8860
His2Av:RFP	Bloomington Stock Center #23651
UAS-Mars RNAi	Bloomington Stock Center #33929
UAS-dgt3 RNAi	Vienna Drosophila Resource Center #103980 (Vienna,
UAS-dgt4 RNAi	AUSTRIA) Vienna Drosophila Resource Center #108969
UAS-dgt6 RNAi	Vienna Drosophila Resource Center #108799
UAS-RCC1 RNAi	Vienna Drosophila Resource Center #110321
UAS-asl RNAi	Vienna Drosophila Resource Center #25457
UAS-sas-6 RNAi	Vienna Drosophila Resource Center #25073
UAS-eiger RNAi	Vienna Drosophila Resource Center #45252,
asl^{mecD}	53,108814.
UAS-bskDN	Blachon et al., 2008
mad2^{P}	Adachi-Yamada et al., 1999
UAS-puc	Buffin et al., 2007
ap-Gal4 UAS-GFP	Martin-Blanco et al., 1998
Jupiter:GFP	Y. Tamori
Polo:GFP	Karpova et al., 2006
TRE-DsRed	Moutinho-Santos et al., 1999
	Chatterjee and Bohmann, 2012

Supplemental References

Adachi-Yamada, T., Nakamura, M., Irie, K., Tomoyasu, Y., Sano, Y., Mori, E., Goto, S., Ueno, N., Nishida, Y. and Matsumoto, K. (1999). p38 mitogen-activated protein kinase can be involved in transforming growth factor beta superfamily signal transduction in Drosophila wing morphogenesis. *Mol Cell Biol* **19**, 2322-2329.

Karpova, N., Bobinnec, Y., Fouix, S., Huitorel, P. and Debec, A. (2006). Jupiter, a new Drosophila protein associated with microtubules. *Cell Motil Cytoskeleton* **63**, 301-312.

Moutinho-Santos, T., Sampaio, P., Amorim, I., Costa, M. and Sunkel, C. E. (1999). In vivo localisation of the mitotic POLO kinase shows a highly dynamic association with the mitotic apparatus during early embryogenesis in Drosophila. *Biol Cell* **91**, 585-596.